

Optimization of Infiltration and Reaction Process for the Production of Strong MgB₂ Bulk Magnets

Arata Ogino, Tomoyuki Naito, and Hiroyuki Fujishiro

Abstract—An infiltration and reaction (IR) process can realize a dense MgB₂ bulk under an ambient pressure, which is preferable for the industrial mass production in cost. However, the trapped field of the IR-processed bulk is commonly rather smaller than that of the high-pressure synthesized bulk, which is caused by the cracks and the thread-like channels of residual Mg preventing the circular supercurrent flow. To obtain the high-quality IR-processed MgB₂ bulk, we investigated the optimization of heat-treatment condition for the IR-process (sintering temperature, $T_{ht} = 700\text{--}900$ °C and holding time, $t_h = 1\text{--}9$ h). A volume fraction of the MgB₂ phase increased monotonically with increasing T_{ht} and/or t_h , and the grain-size increased with increasing T_{ht} . As a result, the highest critical current density J_c and irreversibility field $\mu_0 H_{irr}$ were achieved for the sample sintered at 700 °C for 9 h. The relation between the superconducting properties and the microscopic structure was also discussed.

Index Terms—MgB₂, infiltration and reaction process, critical current density, trapped magnetic field.

I. INTRODUCTION

MgB₂ superconducting bulk magnet realizes highly homogeneous and stable Tesla-class magnetic-field in a compact space [1]–[3]. A cryogenic apparatus equipped with the MgB₂ bulk can be operated in liquid hydrogen due to the superconducting transition temperature, T_c , of 39 K [4]. A simple synthesis process, that is, the sintering of the stoichiometric mixture of Mg and B powders (*in-situ*) or MgB₂ powder (*ex-situ*), is also preferable for the industrial mass production in terms of cost and time. MgB₂ bulk is usually fabricated under a high-pressure to achieve a high filling factor, f , over 90% of the ideal density [4]–[6]. The dense MgB₂ bulk can trap the strong magnetic field over $B_T = 2$ T at 20 K, which is about 1.3 times larger than that of the bulk with $f \sim 50\%$ via the *in-situ*-route under ambient pressure [7]. Contrary to the high-pressure synthesis, an infiltration (diffusion) and reaction (IR) method also realizes the dense bulk ($f > 90\%$) without the external physical pressure [8], [9], in which the liquid Mg infiltrates into and reacts with solid B preform to create MgB₂ above the melting point of Mg, 650 °C. However, the IR-processed MgB₂ bulks generally trap

a magnetic field lower than that of high-pressure synthesized bulks [10]–[12], because the inhomogeneous structures, such as cracks [8] and channels of residual unreacted Mg [12], prevent the circular supercurrent flow, which are caused by the fact that a precise mechanism of infiltration and reaction process has not been investigated in details. Recently, we succeeded the MgB₂ bulk (30 mm in diameter and 6.6 mm in thickness) by IR method with B_T of 2.4 T at 15.9 K (2.1 T at 20.0 K) by suppressing the expansion of the B preform under the liquid Mg-infiltration process using the specially designed home-made capsule [13]. Although the superconducting characteristics are comparable with those of the high-pressure synthesized bulks, this bulk still contained small cracks. And a small amount of Mg₂B₂₅ impurity phase also existed, which is an intermediate product in the IR process but does not prevent supercurrent flowing [14]. However, the creation of Mg₂B₂₅ reduces the superconducting volume fraction and remains the unreacted Mg.

In this paper, we have studied the IR process by observing the formation region of the MgB₂ phase of the samples synthesized for various heat-treatment conditions. We have also discussed the optimal heat-treatment temperature and holding time by using the X-ray diffraction pattern, microstructure, and superconducting properties including T_c , critical current density, J_c and B_T for the MgB₂ phase.

II. EXPERIMENTAL DETAILS

MgB₂ sample was fabricated by an infiltration and reaction process in a closed stainless steel (SUS) tube with 10 mm and 8 mm in outer and inner diameters, respectively, as shown in Fig. 1(a). Raw powders of Mg (99% in purity, ≤ 180 μm in grain size, Kojundo Chemical Laboratory Co., Ltd) and crystalline B (99% in purity, ≤ 45 μm in grain size, Kojundo Chemical Laboratory Co., Ltd) were weighed with Mg : B = 1.1 : 2.0 in molar ratio, in which the excess Mg is expected to compensate the lack of liquid Mg source. The crystalline B powder was firstly poured into the closed-end SUS tube and then pressed using a SUS rod under a uniaxial pressure of 5 MPa in air. The Mg powder was also put and pressed vertically on the B layer in the same way. The height of both B and Mg layers was about 15 mm. The tube was fully sealed using a tube fitting in Ar atmosphere in a glove box. It was fired at $T_{ht} = 700\text{--}900$ °C, which is higher than the melting point of Mg (650 °C), for various holding times, $t_h = 0\text{--}9$ h in the box furnace. A vertical cross-section was cut from the heat-treated objects using a wire electric discharge machine in flowing water.

Manuscript received September 7, 2016; accepted December 2, 2016. Date of publication December 21, 2016; date of current version February 3, 2017. This work was supported in part by the JSPS KAKENHI under Grant JP15K04718 and Grant JP15K04646. (Corresponding author: Tomoyuki Naito.)

The authors are with the Faculty of Science and Engineering, Iwate University, Morioka 020-8551, Japan (e-mail: cloud3254@gmail.com; tnaito@iwate-u.ac.jp; fujishiro@iwate-u.ac.jp).

Color versions of one or more of the figures in this paper are available online at <http://ieeexplore.ieee.org>.

Digital Object Identifier 10.1109/TASC.2016.2643500

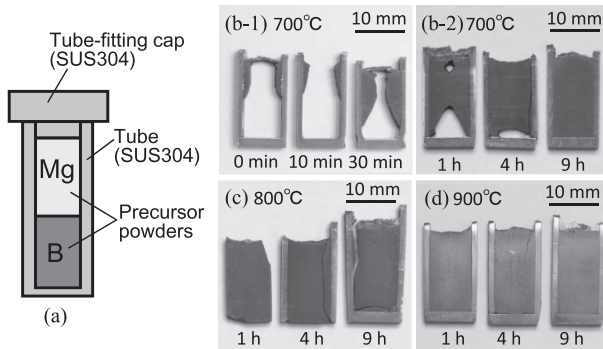


Fig. 1. (a) Schematic image of the precursor powders filled in the closed stainless steel tube. (b)–(d) Pictures of the vertical cross section of the specimens cut from the objects which were heat-treated at (b-1) $T_{ht} = 700^\circ\text{C}$ for $t_h = 0\text{--}30$ min, (b-2) $T_{ht} = 700^\circ\text{C}$ for $t_h = 1\text{--}9$ h, (c) $T_{ht} = 800^\circ\text{C}$ for $t_h = 1\text{--}9$ h, (d) $T_{ht} = 900^\circ\text{C}$ for $t_h = 1\text{--}9$ h.

The constituent phase and crystal structure of the samples were examined by the X-ray diffraction using the Cu- $K\alpha$ radiation (the wave length of 0.154 nm) operated at the acceleration voltage of 30 kV and electron current of 30 mA. Magnetization, M , was measured by a commercial SQUID magnetometer (MPMS-XL, Quantum Design Inc.) as functions of temperature and magnetic field. Critical current density, J_c , was estimated from the magnetic hysteresis loop, $M(\mu_0 H)$, using the extended Bean's critical state model [15], [16]. The temperature dependence of the trapped field, $B_T(T)$, after the field-cooled magnetization was measured by a cryogenic Hall probe (HP-VVP, Arepoc s.r.o) set on the center of the cylindrical bulk surface. Microstructural observation and analysis of chemical composition were performed by a scanning electron microscopy with a field emission electron gun (FE-SEM; JSM-7001F, JEOL Ltd.) coupled with energy dispersive X-ray spectroscopy (EDS) and electron backscatter diffraction (EBSD; NordlysNano, Oxford Instruments plc).

III. RESULTS AND DISCUSSION

Figures 1(b)–(d) show the vertical cross section of the IR-processed samples, in which the outer frame is the SUS tube. An unreacted B precursor probably remained in an empty space found for the 700°C -0-4 h samples, which was removed by the flowing water during the cutting process and a hard reacted material was remained. It should be noticed that the Mg infiltration tends to be promoted from the upper periphery of the Boron layer at $T_{ht} = 700^\circ\text{C}$ for shorter t_h , proceeds also at the central region, and then reaches the bottom of the Boron layer at $t_h = 9$ h, as shown in Fig. 1(b). On the other hand, at $T_{ht} = 800$ and 900°C , the Mg infiltration was completely terminated within $t_h = 1$ h as shown in Figs. 1(c) and 1(d). The IR-process can be clearly observed using this technique.

The XRD pattern was taken at various positions for each sample, as schematically shown in the inset of Fig. 2. The horizontal distance, x , which was measured from the bottom of sample, represents the central position irradiated by the X-ray beam. Figure 2 shows a typical XRD pattern at $x = 8$ mm for the

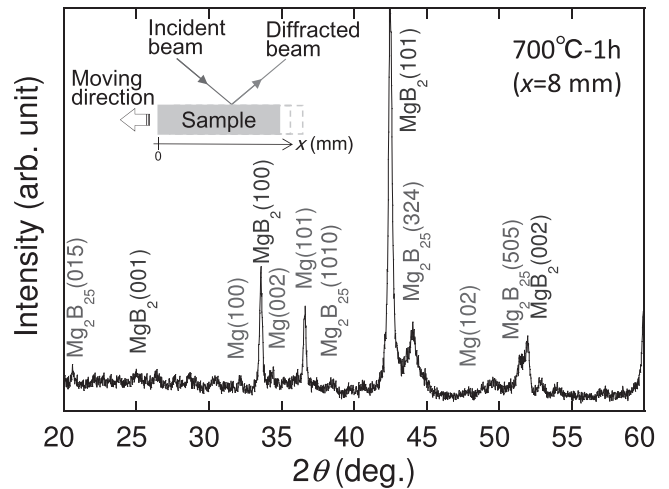


Fig. 2. X-ray diffraction pattern of the 700°C -1h sample, which was measured at $x = 8$ mm of the center of X-ray beam.

700°C -1h sample. The reaction product was confirmed mainly to be MgB_2 with impurities of Mg_2B_{25} and residual unreacted Mg. The similar XRD patterns were obtained for all the samples and at various positions.

Figures 3(a), 3(b) and 3(c), respectively, show the peak intensity of $\text{MgB}_2(101)$ plane, $I_{\text{MgB}_2(101)}$, and the peak intensity ratios of $I_{\text{Mg}_2\text{B}_{25}(324)}/I_{\text{MgB}_2(101)}$ and of $I_{\text{Mg}(101)}/I_{\text{MgB}_2(101)}$, as functions of the heat-treatment temperature, T_{ht} , and holding time, t_h . In Fig. 3(a), the $I_{\text{MgB}_2(101)}$ of about 1,000 cps for the 700°C -1h sample increased to about 2,400 and 3,600 cps for the 800°C -1h and 900°C -1h samples, respectively. The higher $I_{\text{MgB}_2(101)}$ was also obtained for the longer t_h at each T_{ht} . These results suggest that the formation of the MgB_2 phase was promoted with increasing T_{ht} and/or t_h . In Figs. 3(b) and 3(c), the monotonic decrease of both $I_{\text{Mg}_2\text{B}_{25}(324)}/I_{\text{MgB}_2(101)}$ and $I_{\text{Mg}(101)}/I_{\text{MgB}_2(101)}$ can be observed with increasing T_{ht} and elongating t_h , except for the $I_{\text{Mg}(101)}/I_{\text{MgB}_2(101)}$ for 700°C -1h and 800°C -1h samples. These results indicated that the reaction between Mg_2B_{25} and Mg to form the MgB_2 phase was promoted by the heat treatment at higher T_{ht} and for longer t_h .

Figure 4 shows the temperature dependence of the normalized magnetization, $m(T)(=M(T)/M(10\text{ K}))$, for the MgB_2 samples fabricated at $700\text{--}900^\circ\text{C}$ for $t_h = 1$ and 9 h. All the samples, which included the $t_h = 4$ h ones (not shown), showed the sharp superconducting transition around 38 K. Inset shows the critical temperature, T_c^{mid} , at the mid-point ($m = 0.5$) of the transition as functions of the heat-treatment temperature, T_{ht} and the holding time t_h . As shown in the inset, T_c^{mid} tends to be higher at higher T_{ht} and for longer t_h , which is qualitatively consistent with the $I_{\text{MgB}_2(101)}$ behavior shown in Fig. 3(a).

Figure 5 shows the magnetic-field dependence of the critical current density, $J_c(\mu_0 H)$, at $T = 20$ K for the MgB_2 samples fabricated at $700\text{--}900^\circ\text{C}$ for $t_h = 1$ and 9 h. The irreversibility field, $\mu_0 H_{\text{irr}}$, which was defined as a magnetic-field at $J_c = 100\text{ A cm}^{-2}$, of 4.1–4.3 T for the 700°C -samples was evidently

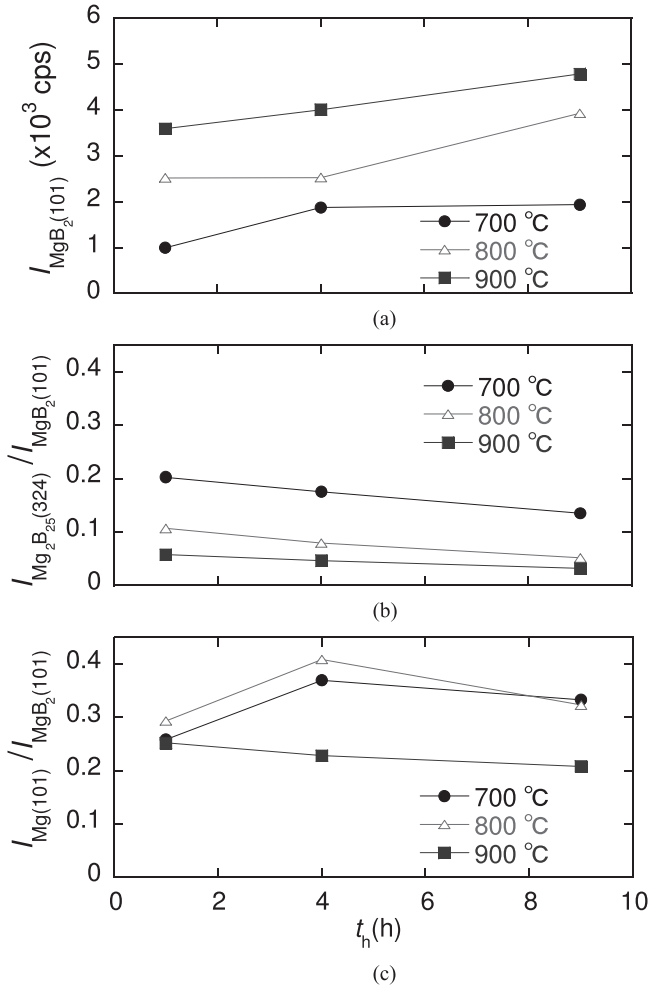


Fig. 3. (a) Peak intensity of MgB₂(101) plane and peak intensity ratios of (b) Mg₂B₂₅(324)/MgB₂(101) and of (c) Mg(101)/MgB₂(101) as functions of the heat-treatment temperature, T_{ht} , and duration time, t_h .

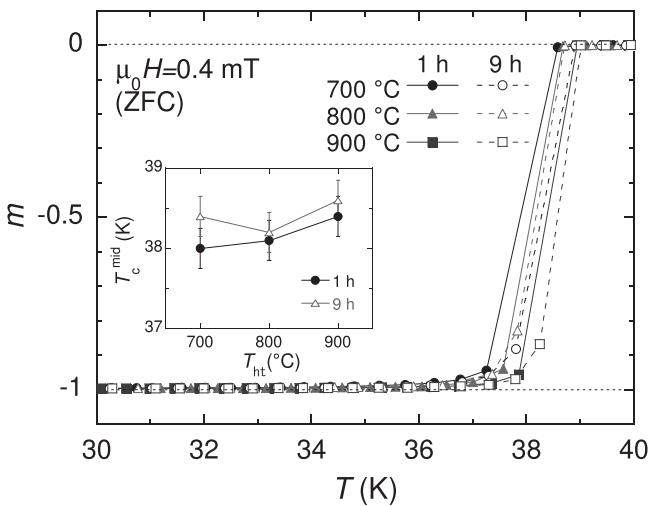


Fig. 4. The temperature dependence of the normalized magnetization, $m(T)$, at $\mu_0 H = 0.4$ mT after zero-field cooling for the MgB₂ samples fabricated at $T_{\text{ht}} = 700, 800$ and 900 °C for $t_h = 1$ h and 9 h. Inset shows the T_c^{mid} vs. T_{ht} plots for the $t_h = 1$ h and 9 h samples.

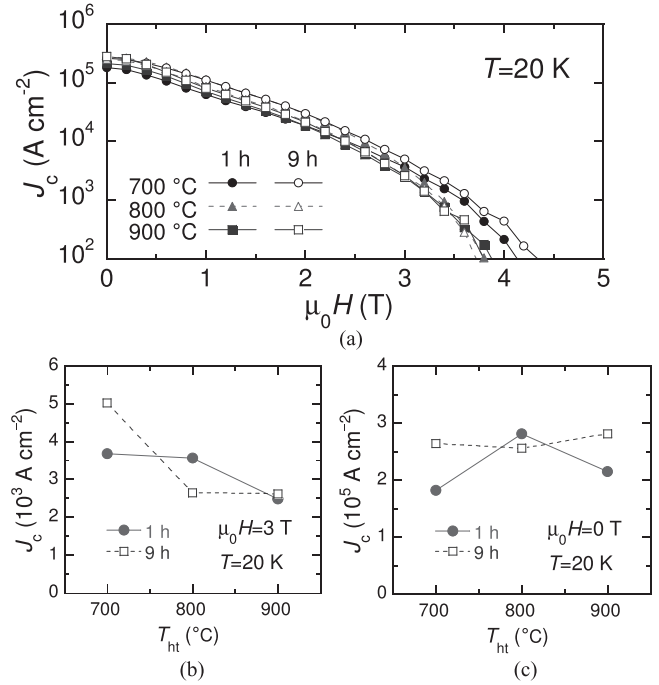


Fig. 5. (a) Magnetic-field dependence of the critical current density, $J_c(\mu_0 H)$, at 20 K for the MgB₂ samples fabricated at 700–900 °C for $t_h = 1$ and 9 h. (b) and (c), respectively, shows the J_c at 20 K under $\mu_0 H = 3$ T and the self-field ($\mu_0 H = 0$ T) as functions of the heat-treatment temperature, T_{ht} and the holding time, t_h .

higher than about 3.8 T for the 800 °C- and 900 °C-samples. The higher J_c under a magnetic field was also realized for the 700 °C-samples; the J_c at 3 T and 20 K was typically shown in Fig. 5(b). On the other hand, the self-field J_c at 20 K was almost independent of the heat-treatment condition, as shown in Fig. 5(c).

Figure 6 shows the secondary electron images (SEI) and the EDS (chemical mapping) images (EDSI) of Mg and B for the 700 °C-1h and 900 °C-9h samples. Both SEI's shown in Figs. 6(a) and 6(b) demonstrated the existence of two distinct light gray and dark gray (LG and DG) regions. A bright area in the EDSI shown in Figs. 6(c)–6(f) represents the existence of the target element. Boron was clearly observed as the absence in the Mg-mapping. Although the surface morphology of the 700 °C-1h sample (Fig. 6(a)) does not reflect the chemical compositions (Figs. 6(c) and 6(e)), the large angular-shaped B particles with small amount of Mg are clearly found, and both Mg and residual B coexisted in the matrix. The quantitative EDS analysis suggested that the large B-enriched particle and the matrix were, respectively, estimated roughly to the Mg₂B₂₅ phase with the unreacted B and the MgB₂ phase with a small amount of B. On the other hand, the DG area in the SEI (Fig. 6(b)) corresponds evidently to the B-enriched particle in the EDSI's (Figs. 6(d) and 6(f)) for the 900 °C-9h sample. These were determined roughly to be the Mg₂B₂₅ phase by the quantitative EDS analysis. The B-enriched particle was rounded and the amount substantially decreased with increasing T_{ht} , indicating that the reaction of liquid Mg and solid B at the periphery of the B particle was

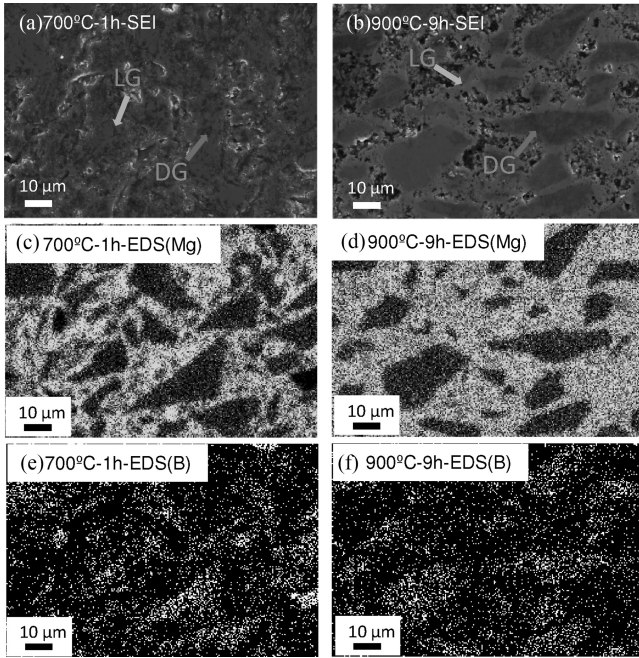


Fig. 6. (a) and (b) the secondary electron images and the chemical mapping images of (c) and (d) Mg and (e) and (f) B for the 700°C-1h and 900°C-9h samples.

promoted by the higher T_{ht} and longer t_h . The grain growth of the MgB_2 was also facilitated for the 900°C-9h sample, because the connected MgB_2 grains can be found in the SEI (Fig. 6(b)).

Figure 7 shows the electron backscattered diffraction images (EBSDI) and EDS images (EDSI) for the 700°C-1h and 700-900°C-9h samples. The EBSD analysis was applied for MgB_2 and Mg phases, which are represented by red and blue colors, respectively. In the EDSI for Mg and B, the bright region shows the existence of the target element. Quite a small amount of nanometer-size MgB_2 grains and quite a large amount of unreacted Mg coexisted with an unanalyzed black-color area in the EBSDI for the 700°C-1h sample (Fig. 7(a-1)). The EDSI's of Mg and B (Figs. 7(a-2) and 7(a-3)) suggest the unreacted B predominantly existed in the black area of EBSDI. As found in the EBSDI of 700°C-9h sample (Fig. 7(b-1)), the creation and grain-growth of MgB_2 were promoted by elongating the holding time, t_h . However the unreacted Mg still substantially remained. Therefore, the longer t_h than 9 h must be required for $T_{ht} = 700$ °C. The MgB_2 grains grew to micrometer-size for the 800°C-9h sample (Fig. 7(c-1)). The amounts of MgB_2 also increased greatly, but at the same time, that of residual Mg decreased for the 800°C-9h sample (Fig. 7(c-1)). The further larger MgB_2 grain with a few micrometer-size was found for the EBSDI of the 900°C-9h sample (Fig. 7(d-1)). In addition, the unreacted Mg still remained, but the unreacted B fully disappeared. These results demonstrate that the existence of fine nanometric MgB_2 grains is preferable to obtain the high $J_c(\mu_0 H)$ and $\mu_0 H_{irr}$, in spite of the quite small volume fraction of MgB_2 .

Figure 8 shows the temperature dependence of the trapped field, $B_T(T)$, of the IR-processed cylindrical bulk (8 mm in

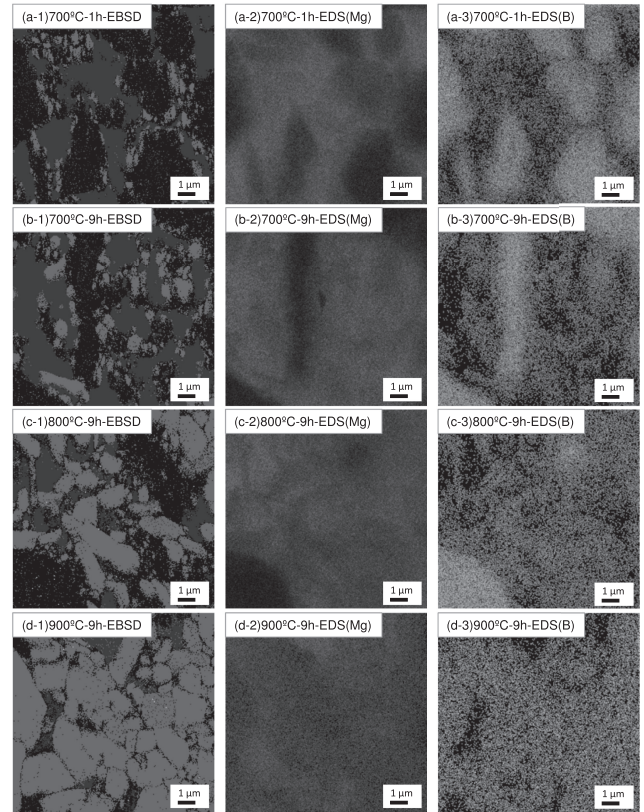


Fig. 7. (a-1) Electron backscattered diffraction (EBSD) image and EDS (chemical mapping) images of (a-2) Mg and (a-3) B for the 700°C-1h sample. (b-), (c-) and (d-) series, respectively, are the same images for the 700 °C, 800 °C and 900 °C samples for $t_h = 9$ h. In the EBSD images, red is MgB_2 and blue is Mg metal. In the EDS images, red is Mg metal and green is B metal.

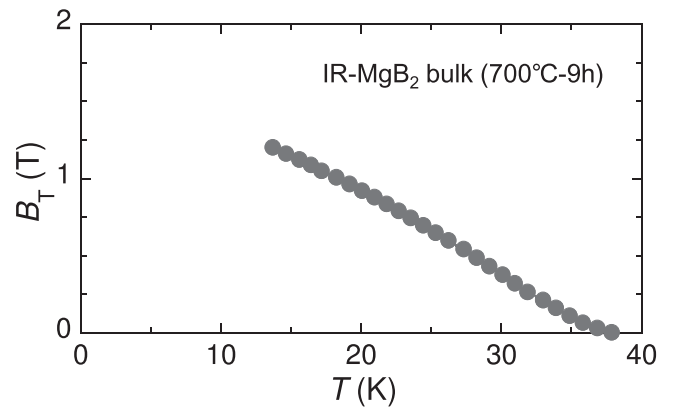


Fig. 8. Temperature dependence of the trapped field, $B_T(T)$, of the IR-processed cylindrical bulk (8 mm in diameter and 15 mm in thickness) synthesized at $T_{ht} = 700$ °C for $t_h = 9$ h.

diameter and 15 mm in thickness) synthesized at $T_{ht} = 700$ °C for $t_h = 9$ h. The highest B_T of 1.2 T was achieved at 13.7 K. The numerical simulation [17] using the $J_c(\mu_0 H)$ of this bulk suggested that this B_T will become approximately twice by enlarging the diameter to 30 mm. The B_T value on the IR-processed MgB_2 bulk become enhanced with increasing both

J_c and the size by the improvement of IR process including the heat-treatment condition and the refinement of B particles.

IV. SUMMARY

We have studied the superconducting properties of the MgB₂ sample fabricated by the infiltration and reaction (IR) process under various heat-treatment conditions (the sintering temperature, $T_{\text{ht}} = 700\text{--}900$ °C and the holding time, $t_h = 0\text{--}9$ h). The observation of IR process suggested that the infiltration process strongly depended on the heat-treatment conditions. An empty region without any hard materials was observed for the samples synthesized at $T_{\text{ht}} = 700$ °C for $t_h = 0\text{--}4$ h. The MgB₂ phase was completely created in the preform under other heat-treatment conditions ($T_{\text{ht}} = 700$ °C for $t_h = 9$ h, $T_{\text{ht}} = 800$ and 900 °C for $t_h \geq 1$ h). The volume fraction of MgB₂ increased with increasing T_{ht} and t_h , and simultaneously the nanometer-size MgB₂ grain for $T_{\text{ht}} = 700$ °C grew to the micrometer-size for $T_{\text{ht}} = 900$ °C. On the other hand, the critical current density, J_c and the irreversibility field, $\mu_0 H_{\text{irr}}$ were degraded for higher T_{ht} . As a result, the MgB₂ sample fabricated at 700 °C for 9 h demonstrated the best performance, $J_c = 5$ kA cm⁻² under 3 T and $\mu_0 H_{\text{irr}} = 4.3$ T at 20 K among the samples studied here. These results suggest that the lower sintering temperature is preferable to obtain the higher vortex pinning properties. Considering the balance of the grain-size with the volume fraction of MgB₂, the optimal t_h seems to be over 9 h for $T_{\text{ht}} = 700$ °C.

ACKNOWLEDGMENT

The authors would like to thank Dr. T. Murakami and Mr. K. Sasaki of Iwate University (IU) for their assistance in microstructural analysis using SEM-EBSD and SEM-EDS apparatuses, and also Mr. Y. Takeda of IU for his help in fabricating the MgB₂ samples.

REFERENCES

- [1] T. Naito, T. Sasaki, and H. Fujishiro, "A proposal of new fabricating technique of large MgB₂ bulk by a capsule method," *IEEE Trans. Appl. Supercond.*, vol. 22, no. 3, Jun. 2012, Art. no. 4401703.

- [2] G. Fuchs *et al.*, "High trapped fields in bulk MgB₂ prepared by hot-pressing of ball-milled precursor powder," *Supercond. Sci. Technol.*, vol. 26, 2013, Art. no. 122002.
- [3] A. Yamamoto, A. Ishihara, M. Tomita, and K. Kishio, "Permanent magnet with MgB₂ bulk superconductor," *Appl. Phys. Lett.*, vol. 105, no. 3, 2014, Art. no. 032601.
- [4] J. Nagamatsu, N. Nakagawa, T. Muranaka, Y. Zenitani, and J. Akimitsu, "Superconductivity at 39 K in magnesium diboride," *Nature*, vol. 410, no. 6824, pp. 63–64, 2001.
- [5] Y. Takano *et al.*, "Superconducting properties of MgB₂ bulk materials prepared by high-pressure sintering," *Appl. Phys. Lett.*, vol. 78, no. 19, pp. 2914–2916, 2001.
- [6] D. Goto, T. Machi, Y. Zhao, N. Koshizuka, M. Murakami, and S. Arai, "Improvement of critical current density in MgB₂ by Ti, Zr and Hf doping," *Physica C*, vol. 392–396, pp. 272–275, 2003.
- [7] T. Sasaki, T. Naito, and H. Fujishiro, "Trapped magnetic field of dense MgB₂ bulks fabricated under high pressure," *Phys. Procedia*, vol. 45, pp. 93–96, 2013.
- [8] G. Giunchi, "High density MgB₂ obtained by reactive liquid Mg infiltration," *Int. J. Mod. Phys. B*, vol. 17, no. 04n06, pp. 453–460, 2003.
- [9] S. Ueda *et al.*, "High critical current properties of MgB₂ bulks prepared by a diffusion method," *Appl. Phys. Lett.*, vol. 86, no. 22, 2005, Art. no. 222502.
- [10] E. Perini, G. Giunchi, L. Saglietti, A. Albisetti, A. Matrone, and V. Cavaliere, "Magnetic field trapping in MgB₂ bulks and inserts," *IEEE Trans. Appl. Supercond.*, vol. 21, no. 3, pp. 2690–2693, 2011.
- [11] H. Mochizuki, H. Fujishiro, T. Naito, A. F. Albisetti, and G. Giunchi, "Trapped field properties of a concentric-circled MgB₂ bulk composite magnetized by pulsed field and field cooling," *Supercond. Sci. Technol.*, vol. 28, no. 10, 2015, Art. no. 105004.
- [12] A. G. Bhagurkar *et al.*, "A trapped magnetic field of 3 T in homogeneous, bulk MgB₂ superconductors fabricated by a modified precursor infiltration and growth process," *Supercond. Sci. Technol.*, vol. 29, no. 3, 2016, Art. no. 035008.
- [13] T. Naito, A. Ogino, and H. Fujishiro, "Potential ability of 3 T-class trapped field on MgB₂ bulk surface synthesized by infiltration-capsule method," *Supercond. Sci. Technol.*, vol. 29, no. 11, 2016, Art. no. 115003.
- [14] G. Giunchi, G. Ripamonti, T. Cavallin, and E. Bassani, "The reactive liquid Mg infiltration process to produce large superconducting bulk MgB₂ manufactures," *Cryogenics*, vol. 46, no. 23, pp. 237–242, 2006.
- [15] C. P. Bean, "Magnetization of hard superconductors," *Phys. Rev. Lett.*, vol. 8, no. 6, pp. 250–253, 1962.
- [16] E. M. Gyorgy, R. B. van Dover, K. A. Jackson, L. F. Schneemeyer, and J. V. Waszczak, "Anisotropic critical currents in Ba₂YCu₃O₇ analyzed using an extended bean model," *Appl. Phys. Lett.*, vol. 55, no. 3, pp. 283–285, 1989.
- [17] H. Fujishiro, T. Naito, and T. Yoshida, "Numerical simulation of the trapped field in MgB₂ bulk disks magnetized by field cooling," *Supercond. Sci. Technol.*, vol. 27, no. 6, 2014, Art. no. 065019.

